International Journal of Heat and Fluid Flow 31 (2010) 227–235

Contents lists available at ScienceDirect

International Journal of Heat and Fluid Flow

journal homepage: www.elsevier.com/locate/ijhff

Simulation of thermal micro-flow using lattice Boltzmann method with Langmuir slip model

Sheng Chen [a,*], Zhiwei Tian [b]

[a] State Key Lab of Coal Combustion, Huazhong University of Science and Technology, Wuhan 430074, China
[b] Department of Coal and Coalbed Methane Engineering, Faculty of Earth Resources, China University of Geosciences, Wuhan 430074, PR China

ARTICLE INFO

Article history:
Received 19 February 2009
Received in revised form 23 November 2009
Accepted 4 December 2009
Available online 6 January 2010

Keywords:
Lattice Boltzmann method
Langmuir slip model
Micro thermal flow

ABSTRACT

We discuss the implementation of the recently developed Langmuir slip model, which possesses a clearer physical picture than the popularly used Maxwell slip model, for the lattice Boltzmann (LB) method to capture velocity slip and temperature jump in microfluidics. The implementation of this scheme is straightforward even when boundary walls do not run coincidentally along the lattice grids. Some previous LB boundary schemes for macroscopic thermal flows can be naturally recovered from the present scheme when the Knudsen number $Kn \to 0$. The feasibility and the capability of the present scheme for thermal micro-flow simulations are explored by numerical experiments.

1. Introduction

With the rapid development of micro- and nano-devices in the last decade, the fluid flow and heat transfer in such devices have received a significant attention (Ho and Tai, 1998; Reese et al., 2003; Darhuber and Troian, 2005). This is largely driven by the need for new theoretical tools to accurately model micro- and nano-scale physical processes and to design devices with enhanced performance. As the different mechanisms behind the complicated phenomenon in such devices are strongly intertwined, the experimental study of a single mechanism is a difficult even impossible task. Therefore, numerical simulations are attractive as they provide a controllable way to change a single property of fluid while keeping the others unchanged.

In micro- and nano-devices, the gas molecular mean free path λ is comparable to the characteristics length H and the micro-flow is usually described by the dimensionless parameter: Knudsen number $Kn = \lambda/H$. Theoretically, when $Kn > 10^{-3}$, the continuum hypothesis, which is the base of the Navier–Stokes (NS) equations, is not valid any more. On the other hand, it is well accepted that the Boltzmann equation can be used to model gas flows ranging from the continuum regime $Kn < 10^{-3}$ to free molecular regime $Kn > 10$ and the direct solver of the full Boltzmann equation is reliable (Reese et al., 2003). Whereas, the required integral computation makes it rather complicated in coding whilst solving the Boltzmann equation directly still remains a formidable challenge. Until now most computer simulations have been performed using the molecular dynamics (MD). For computational reasons the MD is limited to length scales of tens of nanometers and time scales of nanoseconds, which do not comply with the experimentally relevant scales. Traditional numerical approaches for modeling high-speed rarefied flow, such as the direct simulation Monte Carlo (DSMC) method, are very inefficient for flows in micro- and nano-devices because the mathematical difficulties associated with the hypersonic rarefied flow regimes do not appear in microfluidic flows whose speeds are relatively low (Reese et al., 2003).

Recently, the mesoscopic lattice Boltzmann (LB) method developed from kinetic theory has been applied to study microfluidic flows (Nie et al., 2002; Lim et al., 2002; Succi, 2002; Zhang et al., 2005; Lee and Lin, 2005; Ansumali et al., 2006; Ansumali and Karlin, 2005; Sofonea and Sekerka, 2005; Shan et al., 2006; Kunert and Harting, 2007; Niu et al., 2007; Shi et al., 2007; Szalmas, 2006; Verhaeghe et al., 2009; Tang et al., 2008; Kim and Pitsch, 2008; Guo et al., 2008), to cite only a few. Different from MD and DSMC schemes, the LB method is more efficient intuitively in computation because its computational cost is comparable to that of the NS solvers (Chen and Doolen, 1998). More important, it can be applied in wider region theoretically (Succi, 2001). This method allows one to reach experimentally relevant scales and preserves those interactions needed to describe the underlying physics. With its strong theoretical foundation and numerical advantages, the LB method has been taken as an ideal choice for simulating micro-flow dynamic problems where both microscopic and macroscopic behavior are important (Succi, 2001; Tian et al., 2007).

* Corresponding author.
E-mail addresses: shengchen.hust@gmail.com (S. Chen), zwtian@cug.edu.cn (Z. Tian).

0142-727X/$ - see front matter © 2009 Elsevier Inc. All rights reserved.
doi:10.1016/j.ijheatfluidflow.2009.12.006

To date available open literature is mostly concerned with the isothermal micro-flow. However, the studies using the LB method on the thermal counterpart are quite sparse (Tian et al., 2006, 2007; Sofonea and Sekerka, 2005; Shu et al., 2005; Wang and Yang, 2006; Zhang et al., 2007; Kao et al., 2008). Sofonea and Sekerka (2005) focused on the implementation of diffuse reflection boundary conditions for a thermal finite difference LB model with multiple speeds. Two series of relaxation time expressions (constant and density dependent) were performed, compared with the analytical velocity and temperature profiles. Flow and heat transport were divided into two cases in simulation. Stationary heat transport between two planes at rest was studied without the influence of flow. Moreover, an extra factor (1.15 is chosen) had to be added to obtain better capture of the slip velocity. In Shu et al. (2005), based on the kinetic theory and thermal LB model, a diffuse-scattering boundary condition treatment was presented to capture the velocity slip and temperature jump at wall boundaries. Wang and Yang (2006) also studied micro-scale thermal flow using an independent distribution function to simulate the temperature evolution, and analyzed the two-dimensional heat transfer character in micro-channels with different Kn. Tian and his cooperators developed a scheme based on He's thermal LB model (He et al., 1998) to describe the effect of viscous heat dissipation in microfluidics. They validated their scheme by thermal micro-Poiseuille flow (Tian et al., 2007) and thermal micro-Couette flow (Tian et al., 2006). In their work it was showed that Kn is a parameter describing the character of micro-flow fluid, while the temperature jump depends on the property of heat transfer much more. Kao et al. used the lattice Bhatnagar–Gross–Krook (BGK) model with the Boussinesq approximation to investigate mesoscopic natural convection in rectangular cavities (Kao et al., 2008). The simulation results showed that unstable flow was generated at particular values of the Rayleigh number, Knudsen number, and cavity aspect ratio. More recently, in Zhang et al. (2007) the LB method was extended to simulate thermal micro-flow within the transition regime by Zhang and his cooperators. In their model, a correction function was introduced to account for the reduction in the mean free path near a wall.

As the device size shrinks to the micro-scale, the physics at solid surfaces play a critical role in microfluidic transport since the relative importance of surface forces increases, for example, the van der Waals force in the interaction of gas molecules and surface atoms (Myong et al., 2005). Modeling the molecular interaction between gas particles and the solid-surface atoms is accomplished by a boundary condition in any computational approach. Consequently, to employ LB models in simulation of micro-flows, the most important key issue is how to treat the slip (jump) boundary condition (Tian et al., 2007; Zhang et al., 2007; Kuo and Chen, 2008). In almost all existing studies with the LB method, the Maxwell model (Maxwell, 1879) is popularly used in slip boundary conditions to describe the slip phenomenon in rarefied gas flow. The velocity slip (temperature jump) in the Maxwell model is determined by the accommodation coefficients, Knudsen number, and the gradient of velocity (temperature). The main disadvantage of the Maxwell model lies in the fact that the choices of the accommodation coefficients, which just are free parameters based on the concept of diffusive reflection, have a large impact on the final results (Kim et al., 2007). The so-called Reynolds analogy between heat transfer and momentum transfer was not longer preserved in the Maxwell model (Myong et al., 2006). Furthermore, it was reported that the slip velocity can become unbounded in certain case (Choi et al., 2005; Kim et al., 2007). And the results obtained by the Maxwell model may deviate significantly with the benchmark values (Kim et al., 2007).

Recently, Myong (2004), Myong et al. (2006) developed a new slip model based on the theory of adsorption phenomena pioneered by Langmuir (1933). According to Langmuir's theory, gas molecules do not reflect directly, but rather reside on the surface for a brief period of time due to the intermolecular forces between the gas molecules and the surface atoms. After some lag in time, these molecules may reflect from the surface. This time lag causes macroscopic velocity slip. This new model, named as "the Langmuir slip model" in which the information on the shear stress or velocity gradient at the wall is not required, has been successfully applied to several flow problems of interest (Myong et al., 2005, 2006). Furthermore, it has been shown that this Langmuir slip model recovers the Maxwell model in its first-order approximation and therefore a physical meaning can now be assigned to the accommodation coefficients in the Maxwell model (Myong et al., 2005).

But surprising, there is no attempt to introduce the Langmuir slip model into the LB method for thermal micro-flow simulations. To the best knowledge of the present authors, to date there is only two publications (Kim et al., 2007; Chen and Tian, 2009) on using the LB method with the Langmuir slip model for microfluidics. In Kim et al. (2007), the authors showed how to implement the Langmuir slip model by bounce-back scheme. However, the transformation matrixes in the scheme are complicated, especially for 3D problems, and can hardly be extended for curvilinear walls (Kim et al., 2007). Chen and Tian (2009) also designed a boundary scheme based on the Langmuir slip model, but their discussion is limited in isothermal cases.

In the present study, we discuss a simple implementation of the Langmuir slip model for the LB method to simulate micro-flow with temperature difference. For convenience, a LB model for thermal micro-flow recently developed by the present authors (Tian et al., 2007) is employed in the present study. The implementation of this scheme is straightforward and some existing LB boundary schemes for macroscopic thermal flows (Chen and Krafczyk, 2009; Chen et al., 2007; Tang et al., 2005) can be naturally recovered from the present scheme when $\mathrm{Kn} \to 0$. The feasibility and the capability of the present scheme for thermal micro-flow simulations are explored by numerical experiments.

The rest of the paper is organized as follows. The LB model for thermal micro-flow is briefly reviewed in Section 2. In Section 3, the implementation of Langmuir slip model is introduced, together with a brief comment on the shortcoming of Maxwell slip model. Results and discussion are presented in Section 4. Conclusion is made in the last section.

2. Thermal LB Model for micro-flow

2.1. Evolving equations

The evolving equations of the LB model for micro-flow with temperature difference developed in our previous work (Tian et al., 2006, 2007), which based on He's model (He et al., 1998) to describe the effect of viscous heat dissipation in micro-flow, read:

$$\tilde{f}_i(\mathbf{x}+\mathbf{c}_i\triangle t, t+\triangle t)-\tilde{f}_i(\mathbf{x},t)=-\frac{\triangle t}{\tau_f+0.5\triangle t}[\tilde{f}_i(\mathbf{x},t)-f_i^{eq}(\mathbf{x},t)] \quad (1)$$

$$\tilde{g}_i(\mathbf{x}+\mathbf{c}_i\triangle t, t+\triangle t)-\tilde{g}_i(\mathbf{x},t) = -\frac{\triangle t}{\tau_g+0.5\triangle t}[\tilde{g}_i(\mathbf{x},t)-g_i^{eq}(\mathbf{x},t)]-\frac{\tau_g\triangle t}{\tau_g+0.5\triangle t}f_i Z_i \quad (2)$$

In the LB model, each evolving equation of Eqs. (1) and (2) consists of two computational steps

$$\text{collision}: \quad \tilde{f}_i^{+}(\mathbf{x},t) = (1-\eta_f)\tilde{f}_i(\mathbf{x},t) + \eta_f f_i^{eq}(\mathbf{x},t),$$
$$\text{streaming}: \quad \tilde{f}_i(\mathbf{x}+\mathbf{c}_i\Delta t, t+\Delta t) = \tilde{f}_i^{+}(\mathbf{x},t), \tag{3}$$
$$\text{collision}: \quad \tilde{g}_i^{+}(\mathbf{x},t) = (1-\eta_g)\tilde{g}_i(\mathbf{x},t) + \eta_g g_i^{eq}(\mathbf{x},t) - \eta_g\tau_g f_i Z_i,$$
$$\text{streaming}: \quad \tilde{g}_i(\mathbf{x}+\mathbf{c}_i\Delta t, t+\Delta t) = \tilde{g}_i^{+}(\mathbf{x},t), \tag{4}$$

where $\eta_f = \frac{\triangle t}{\tau_f + 0.5\triangle t}$ and $\eta_g = \frac{\triangle t}{\tau_g + 0.5\triangle t}$.

The new variables $\tilde{f}_i$ and $\tilde{g}_i$ are defined as followed:

$$\tilde{f}_i = f_i + \frac{0.5\triangle t}{\tau_f}(f_i - f_i^{eq}) \tag{5}$$

$$\tilde{g}_i = g_i + \frac{0.5\triangle t}{\tau_g}(g_i - g_i^{eq}) + 0.5\triangle t f_i Z_i \tag{6}$$

where f_i and g_i are the density distribution function and internal energy density distribution function in the ith direction, respectively; $\triangle x$ and $\triangle t$ are the lattice grid spacing and the time step; τ_f and τ_g are the momentum and internal energy relaxation time; f_i^{eq} and g_i^{eq} are their corresponding equilibrium functions, for two-dimensional nine-directional (D2Q9) square lattice (Fig. 1) with $c = \sqrt{3R\overline{T}}$ (where $\overline{T}$ is the average temperature and R is the universal gas constant), the equilibrium (internal energy) density distributions are chosen as:

$$f_i^{eq} = \omega_i\rho\left[1 + \frac{3(\mathbf{c}_i\cdot\mathbf{u})}{c^2} + \frac{9(\mathbf{c}_i\cdot\mathbf{u})^2}{2c^4} - \frac{3(\mathbf{u}\cdot\mathbf{u})}{2c^2}\right] \tag{7}$$

$$g_i^{eq} = \begin{cases} \omega_i\rho e(-\frac{3(\mathbf{u}\cdot\mathbf{u})}{2c^2}), & (i=0) \\ \omega_i\rho e[1.5 + \frac{3(\mathbf{c}_i\cdot\mathbf{u})}{2c^2} + \frac{9(\mathbf{c}_i\cdot\mathbf{u})^2}{2c^4} - \frac{3(\mathbf{u}\cdot\mathbf{u})}{2c^2}], & (i=1\text{–}4) \\ \omega_i\rho e[3 + \frac{6(\mathbf{c}_i\cdot\mathbf{u})}{c^2} + \frac{9(\mathbf{c}_i\cdot\mathbf{u})^2}{2c^4} - \frac{3(\mathbf{u}\cdot\mathbf{u})}{2c^2}], & (i=5\text{–}8) \end{cases} \tag{8}$$

with the weight factors: $\omega_0 = 4/9$, $\omega_{1-4} = 1/9$, and $\omega_{5-8} = 1/36$. And the internal energy density is $\rho e = \rho RT$ (in 2D), $\mathbf{c}_i$ is the particle discrete velocity, for square lattice model:

$$\mathbf{c}_i = \begin{cases} (0,0), & (i=0) \\ (\cos(i-1)\pi/2,\ \sin(i-1)\pi/2)c, & (i=1\text{–}4) \\ \sqrt{2}(\cos(i-5)\pi/2+\pi/4,\ \sin(i-5)\pi/2+\pi/4)c, & (i=5\text{–}8) \end{cases} \tag{9}$$

The term $Z_i = (\mathbf{c}_i - \mathbf{u})\cdot[\partial\mathbf{u}/\partial t + (\mathbf{c}_i\cdot\nabla)\mathbf{u}]$ represents the effect of viscous heating and can be expressed as (Tian et al., 2006, 2007):

$$Z_i = \frac{(\mathbf{c}_i - \mathbf{u})\cdot[\mathbf{u}(\mathbf{x}+\triangle\mathbf{x}, t+\triangle t) - \mathbf{u}(\mathbf{x},t)]}{\triangle t} \tag{10}$$

And the macroscopic density ρ, velocity $\mathbf{u}$, internal energy per unit mass e, kinematic viscosity ν_f, and thermal diffusivity D can then be obtained from the following equations (Tian et al., 2006):

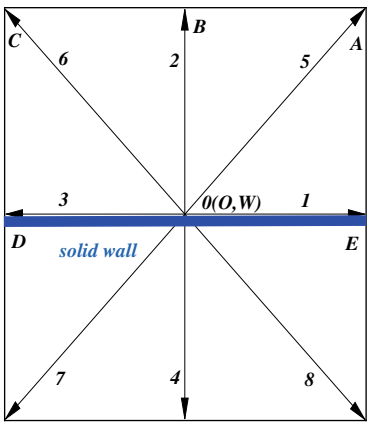

Fig. 1. Schematic plot of the D2Q9 lattice at a wall boundary.

$$\rho = \sum_i \tilde{f}_i \quad \rho\mathbf{u} = \sum_i \mathbf{c}_i\tilde{f}_i \quad \rho e = \sum_i \tilde{g}_i - 0.5\triangle t\sum_i f_i Z_i$$
$$\nu_f = \tau_f c_s^2 \quad D = 2\tau_g c_s^2$$

where $c_s^2 = c^2/3$.

2.2. Relaxation time and Knudsen number

In order to simulate the micro-flow by the LB method, the first step is to define the relation between the Knudsen number Kn and the relaxation time τ. As we know, in the kinetic theory, the kinematic viscosity is $\nu_f = 0.5\bar{c}\lambda$ (where the mean molecule velocity $\bar{c} = \sqrt{8RT/\pi}$). Combined with the kinematic viscosity expression of the LB method, we can gain the final simplified relation for the standard D2Q9 lattice BGK model (Tian et al., 2006, 2007):

$$\mathrm{Kn} = \sqrt{\frac{\pi}{6}}\cdot\frac{\tau}{H\triangle t} \tag{11}$$

No free parameter needs to be adjusted in order to produce desirable simulation results in this model. Here, we need to emphasize that the Knudsen number relation expression differs among various lattice models. The detailed discussion can be found in Tian et al. (2007, 2006) and references therein.

3. Langmuir model for velocity slip and temperature jump boundary condition

3.1. Maxwell slip model

The idea of the Maxwell model is to make a correction of slip based on the degree of nonequilibrium near the wall surface which can best be represented via the shear stress (Maxwell, 1879). The following slip (jump) boundary condition is proposed:

$$u^{slip} = \sigma\mathrm{Kn}\left(\frac{\partial u}{\partial y}\right)_w, \tag{12}$$
$$T^{jump} = \phi\left(\frac{2\gamma}{\gamma+1}\right)\left(\frac{\mathrm{Kn}}{\mathrm{Pr}}\right)\left(\frac{\partial T}{\partial y}\right)_w,$$

where γ is the specific heat ratio and Pr is the Prandtl number. $\sigma = \frac{2-\sigma_v}{\sigma_v}$ and $\phi = \frac{2-\phi_T}{\phi_T}$; the tangential-momentum-accommodation coefficient σ_v is defined as the fraction of molecules reflected diffusively, and ϕ_T is the thermal-accommodation coefficient. It is clear that the accommodation coefficients in the Maxwell model do not depend explicitly on the properties at wall, such as wall temperature. In practical simulations, the values of these two coefficients are chosen according to available results obtained by other means, for example, from experimental data (Tian et al., 2007; Sofonea and Sekerka, 2005; Myong et al., 2005). There are two problems may hinder the applications of this model: first, in most situations we have no prior knowledge on what the values of accommodation coefficients should be (Reese et al., 2003; Myong, 2004), and second, when the temperature jump is taken into account, a more complicated picture is revealed: that heat transfer can increase or decrease with increasing rarefaction, depending on the ratio of thermal accommodation to momentum accommodation, so the Reynolds analogy between heat transfer and momentum transfer is not preserved any more (Myong et al., 2006).

3.2. Langmuir slip model

An alternative approach to describe the slip (jump) can be developed by taking into account the interfacial interaction between the gas molecules and the surface atoms. In this approach the gas molecules are assumed to interact with the surface of the solid via a long range attractive force. Consequently the gas

molecules can be adsorbed onto the surface, and then desorbed after some time lag. This mechanism of the deposition of a layer with a thickness of one or more molecules onto the surface is known as adsorption in the literature of surface chemistry (Langmuir, 1933). One can model this interaction as a chemical reaction in which the gas molecule, m, and the site, s, form the complex, c, we may obtain an expression for the fraction of the surface covered by adsorbed atoms at thermal equilibrium, α:

$$\alpha = \frac{\beta p}{1+\beta p} \tag{13}$$

for monatomic gases and

$$\alpha = \frac{\sqrt{\beta p}}{1+\sqrt{\beta p}} \tag{14}$$

for diatomic gases. Where

$$\beta = \frac{K}{k_B T_w}, \quad K = \frac{C_c}{C_m C_s}$$

and p is the pressure. k_B is the Boltzmann constant. The equilibrium constant, K, which are functions of the concentrations $C_{m,s,c}$ and the wall temperature T_w. As the pressure increases, the value of α approaches unity, implying that most of the molecules are at thermal equilibrium (Myong et al., 2006).

With information about the fraction of the surface covered at equilibrium determined by this adsorption isotherm, in the Langmuir slip model the velocity slip and temperature jump can be expressed as (Myong, 2004; Myong et al., 2006):

$$\begin{aligned} u^{slip} &= (1-\alpha)u_g + \alpha u_w \\ T^{jump} &= (1-\alpha)T_g + \alpha T_w \end{aligned} \tag{15}$$

where the subscript w denotes a local value at the wall. And g represents that adjacent to the wall, for example, a mean free path away from the wall, or a reference value such as the free-stream condition (Myong et al., 2006). In the incompressible limit β takes the form (Myong, 2004):

$$\beta = \frac{A\lambda}{k_B T_w \mathrm{Kn}} exp\left(\frac{D_e}{k_B T_w}\right) = \frac{1}{4\omega \mathrm{Kn}} \tag{16}$$

where A the mean area of a site and

$$\begin{aligned} \omega &= \omega_0(v)\left(\frac{T_w}{T_r}\right)^{1+2/(v-1)} exp\left(-\frac{D_e}{k_B T_w}\right), \\ \omega_0(v) &= \frac{8\sqrt{2}}{5\pi} A_2(v)\Gamma\left[4-\frac{2}{v-1}\right] \end{aligned} \tag{17}$$

where the subscript r denotes a reference value. v is the exponent of the inverse power laws. D_e, whose value varies with the type of gas and the nature of the wall material, is the potential energy of heat adsorption. The detailed values of D_e, $A_2(v)$, and $\omega_0(v)$ can be found in Myong et al. (2006). The role of the coefficient ω, which is a function of v, T_w, and D_e, is very similar to the slip coefficient, σ, in the Maxwell model but its value can be determined with a clear physical explanation prior to simulations (Myong et al., 2005).

3.3. Implementation of Langmuir slip model in the LB method

The task of boundary treatment is to evaluate the virtual unknown (internal energy) density distribution function coming from outside the flow domain before the streaming step (Chen and Doolen, 1998). Usually the bounce-back scheme is employed, not only for macroscopic hydrodynamics (Chen and Doolen, 1998) but also for microfluidics (Kim et al., 2007). However, this scheme is originally designed for flat walls, and when used for curved walls, the boundaries must be represented by lattice nodes. As a result, the boundaries usually become jagged and will introduce some additional errors (Chen and Krafczyk, 2009).

In this section we design a different strategy to implement the Langmuir slip model for the LB method. For simplicity, we consider the case of a flat boundary in which grid nodes are located, namely the solid wall node w overlaps with the boundary node O, as Fig. 1 illustrates. The DOE line lies at the boundary, and the nodes A, B, and C are those lying in the fluid. At the boundary node O, before streaming step, the (internal energy) density distribution functions in $\mathbf{c}_2, \mathbf{c}_5$, and $\mathbf{c}_6$ directions (i.e. $\tilde{f}^+_{2,5,6}$ and $\tilde{g}^+_{2,5,6}$) are unknown and must be closed by the boundary scheme. Following we take $\tilde{f}^+_2$ and $\tilde{g}^+_2$ as the representatives for illustration and the others can be handled in the same way.

According to the Chapman–Enskog method, the (internal energy) density distribution function can be decomposed into its equilibrium and nonequilibrium parts (Chen and Doolen, 1998):

$$\begin{aligned} \tilde{f}_i(\mathbf{x},t) &= f_i^{eq}(\mathbf{x},t) + f_i^{neq}(\mathbf{x},t), \\ \tilde{g}_i(\mathbf{x},t) &= g_i^{eq}(\mathbf{x},t) + g_i^{neq}(\mathbf{x},t), \end{aligned} \tag{18}$$

where the superscript neq denotes the nonequilibrium part of the (internal energy) density distribution function. Thus the post-collision (internal energy) density distribution function in $\mathbf{c}_2$ direction at the boundary node O can be assumed as (Tang et al., 2005)

$$\begin{aligned} \tilde{f}_2{}^+(O,t) &= F_2^{eq}(O,t) + (1-\eta_f)F_2^{neq}(O,t), \\ \tilde{g}_2{}^+(O,t) &= G_2^{eq}(O,t) + (1-\eta_g)G_2^{neq}(O,t) - \eta_g \tau_g f_2 Z_2, \end{aligned} \tag{19}$$

In conformity to the Langmuir model Eq. (15), the natural choices for $F_2^{eq}(O,t)$ and $G_2^{eq}(O,t)$ are

$$\begin{aligned} F_2^{eq}(O,t) &= \alpha f_2^{eq}(W,t) + (1-\alpha) f_2^{eq}(B,t), \\ G_2^{eq}(O,t) &= \alpha g_2^{eq}(W,t) + (1-\alpha) g_2^{eq}(B,t), \end{aligned} \tag{20}$$

and

$$\begin{aligned} F_2^{neq}(O,t) &= \alpha f_2^{neq}(W,t) + (1-\alpha) f_2^{neq}(B,t), \\ G_2^{neq}(O,t) &= \alpha g_2^{neq}(W,t) + (1-\alpha) g_2^{neq}(B,t), \end{aligned} \tag{21}$$

First we discuss how to calculate the equilibrium parts, namely Eq. (20). At time t, the macroscopic quantities of the flow, such as velocity, temperature, and mass density, are known at the fluid node B, so the equilibrium part of (internal energy) density distribution function (i.e. $f_2^{eq}(B,t)$ and $g_2^{eq}(B,t)$) can be determined straightforwardly. For $f_2^{eq}(W,t)$ and $g_2^{eq}(W,t)$, with the velocity and temperature condition in which $\mathbf{u}(W,t)$ and $T(W,t)$ are known but $\rho(W,t)$ is unknown, the approximation proposed in Refs. (Tang et al., 2005, 2007; Chen and Krafczyk, 2009) is adopted

$$\begin{aligned} f_2^{eq}(W,t) &= f_2^{eq}(\rho(B), \mathbf{u}(W), T(W), t) + \mathcal{O}(\varepsilon^2), \\ g_2^{eq}(W,t) &= g_2^{eq}(\rho(B), \mathbf{u}(W), T(W), t) + \mathcal{O}(\varepsilon^2), \end{aligned} \tag{22}$$

where ε is a slight quantity (Tian et al., 2007).

Now we discuss the determination of the nonequilibrium parts $F_2^{neq}(O,t)$ and $G_2^{neq}(O,t)$. The nonequilibrium parts of the distributions at node B can be given by

$$\begin{aligned} f_2^{neq}(B,t) &= f_2(B,t) - f_2^{eq}(B,t), \\ g_2^{neq}(B,t) &= g_2(B,t) - g_2^{eq}(B,t), \end{aligned} \tag{23}$$

Note that $f_2^{neq}(W,t) = f_2^{neq}(B,t) + \mathcal{O}(\varepsilon^2)$ and $g_2^{neq}(W,t) = g_2^{neq}(B,t) + \mathcal{O}(\varepsilon^2)$ (Tang et al., 2005, 2007; Chen and Krafczyk, 2009), so $f_2^{neq}(W,t)$ and $g_2^{neq}(W,t)$ can be approximated by a first-order extrapolation

$$\begin{aligned} f_2^{neq}(W,t) &= f_2(B,t) - f_2^{eq}(B,t) + \mathcal{O}(\varepsilon^2), \\ g_2^{neq}(W,t) &= g_2(B,t) - g_2^{eq}(B,t) + \mathcal{O}(\varepsilon^2), \end{aligned} \tag{24}$$

Eq. (24) implies that the accuracy of the approximation of $f_2^{neq}(W,t)$ ($g_2^{neq}(W,t)$) with the first-order extrapolation scheme based on $f_2^{neq}(B,t)$ ($g_2^{neq}(B,t)$) is indeed of second-order.

With the aid of Eqs. (23) and (24), Eq. (21) reduces

$$F_2^{neq}(O,t) = f_2(B,t) - f_2^{eq}(B,t) + \mathcal{O}(\varepsilon^2), \qquad (25)$$
$$G_2^{neq}(O,t) = g_2(B,t) - g_2^{eq}(B,t) + \mathcal{O}(\varepsilon^2),$$

Therefore, according to Eqs. (20) and (25),the final expression of Eq. (19) reads:

$$\tilde{f}_2^{+}(O,t) = \alpha f_2^{eq}(\rho(B),\mathbf{u}(W),T(W),t) + (1-\alpha)f_2^{eq}(B,t) + (1-\eta_f)[f_2(B,t) - f_2^{eq}(B,t)] + \mathcal{O}(\varepsilon^2), \qquad (26)$$
$$\tilde{g}_2^{+}(O,t) = \alpha g_2^{eq}(\rho(B),\mathbf{u}(W),T(W),t) + (1-\alpha)g_2^{eq}(B,t) + (1-\eta_g)[g_2(B,t) - g_2^{eq}(B,t)] - \eta_g\tau_g f_2(W,t)Z_2(W,t) + \mathcal{O}(\varepsilon^2),$$

The pressure boundary condition(heat flux boundary condition), in which the pressure $p(W,t)$(heat flux q) is known instead of $\mathbf{u}(W,t)$ (temperature T), can be handled in the same way. The details can be found in Tian et al. (2007); Chen et al. (2007); Tang et al. (2005) and the references therein.

When Kn $\to$ 0, namely $\alpha \to 1$ (see Eqs. (13) and (16)), the previous LB boundary schemes for macroscopic thermal flows (Chen and Krafczyk, 2009; Chen et al., 2007; Tang et al., 2005) can be recovered naturally from the present scheme. Furthermore, there are two additional obvious advantages of the present scheme: First, although its formation is first-order extrapolation, this scheme possesses second-order accuracy, so both computational stability and numerical accuracy are preserved, and second, the implementation of this scheme is straightforward and can be easily extended for curved walls (Tang et al., 2005; Guo et al., 2002).

If the solid wall node w does not overlap with the boundary node O, Eq. (26) has to be modified slightly. We will show the modification in the next section by an instance.

4. Numerical results

In order to validate the present scheme, two-dimensional planar thermal micro-Couette flows with different temperature boundary conditions are simulated with variable Kn. Two infinite parallel plates are separated by a distance $H = 1.0$. The upper plate at $y = H$ moves at a constant velocity $U_0 = 0.1c$, while the bottom plate is at rest. Their temperatures are T_{w1} and T_{w0}, respectively, and the average temperature is $\overline{T} = 0.5(T_{w1} + T_{w0})$. $\omega = 1/4$ and $p = 1.0$ are chosen to evaluate α through Eq. (13). Periodic boundary conditions are applied at the inlet and outlet of the channel. In the simulation, we assume that the density and temperature variations across the channel are small enough for the value of the Knudsen number to be considered constant and the vertical velocity is zero everywhere. In this case, the non-dimensionalized density ρ, temperature T and velocity fields depend only on the y coordinate. And the thermal creep term, which is generated by the temperature gradient along x direction, can be also neglected. The whole computational domain is discretized with uniform square grids.

According to above assumptions, the analytical solutions of velocity and temperature profiles with viscous heat dissipation read (Tian et al., 2006):

$$u(y) = U_0\frac{y/H + \mathrm{Kn}}{1 + 2\mathrm{Kn}} \qquad (27)$$
$$T(y) = C_0\left(\frac{y}{H}\right)^2 + C_1\left(\frac{y}{H}\right) + C_2 \qquad (28)$$

where $C_0 = -0.5\tilde{U}_0^2\mathrm{Pr}$, $C_1 = 0.5\tilde{U}_0^2\mathrm{Pr} + \frac{T_{w1}-T_{w0}}{2\mathrm{Kn}+1}$, $C_2 = T_{w0} + \mathrm{Kn}\cdot C_1$ and $\tilde{U}_0 = U_0/(1+2\mathrm{Kn})$.

4.1. Micro-Couette flow with constant wall temperature

The first case is the micro-Couette flow with constant wall temperature boundary condition ($T_{w1} = T_{w0} = T_w = 1.0$). The initial fluid velocity is zero and temperature is equal to the wall temperature T_w. In order to obtain grid-independent results, in the present study, four different grid resolutions 20×20, 30×30, 40×40, and 60×60 are used. As Table 1 shows, the grid resolution 40×40 is fine enough for the present simulation. For the first case, c is determined by

$$c = \sqrt{3T_w} \qquad (29)$$

Figs. 2 and 3 show the linear velocity profile and the parabolic temperature profiles, respectively, with Kn varying from 0.01 to 0.1. The three curves represent Kn = 0.01, 0.05, and 0.1, respectively. The solid lines are analytical results and the scatter points are numerical

Table 1
Temperature jump at the top wall with different grid resolutions and Kn = 0.1.

20×20	30×30	40×40	60×60	Analytical solution
0.001207	0. 001208	0. 001209	0. 001209	0. 001215

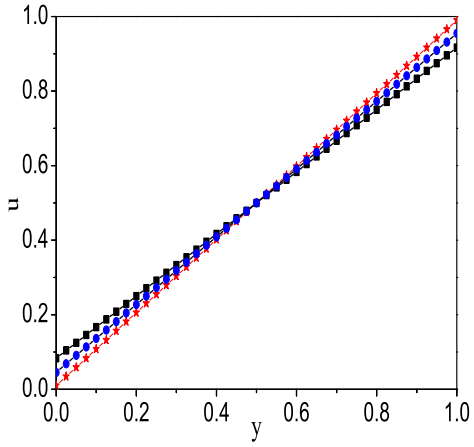

Fig. 2. Velocity profile: solid line, analytical solution; pentacle, Kn = 0.01; dot, Kn = 0.05; square, Kn = 0.1.

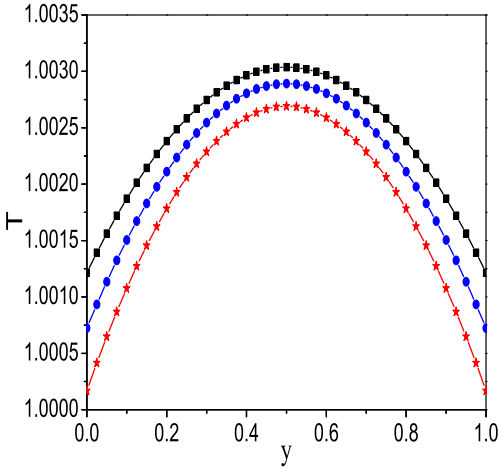

Fig. 3. Temperature profile: solid line, analytical solution; pentacle, Kn = 0.01; dot, Kn = 0.05; square, Kn = 0.1.

simulation results. All of them are matched pretty well. We also find the velocity slip and temperature jump at the boundary increase with Kn increasing, which agree with that in Tian et al. (2006).

Fig. 4 illustrates the convergence behavior of the present model with different grid resolutions and Kn. The slopes of straight lines in Fig. 4 are 1.95 (line of Kn = 0.1), 1.97 (line of Kn = 0.05) and 1.96 (line of Kn = 0.01). The relative global error is measured at the steady state between the numerical solution and the analytical solution u^* given by Eq. (27) and is defined by

$$U_{Error} = \frac{\Sigma_\Omega |u - u^*|}{\Sigma_\Omega |u^*|} \tag{30}$$

where the subscript Ω means the whole computational domain. The data demonstrate that the accuracy of the present model is second-order indeed.

In this validation section, we consider the situation that the solid wall node w does not overlap with the lattice node O. As shown in Fig. 5, the stationary solid wall cuts across the lattice links with distance $\triangle = \frac{x_f - x_w}{x_f - x_b}$. There are many publications (Guo et al., 2002; Fillipova and Hanel, 1998; Mei et al., 1999; Chun and Ladd, 2007) discussing how to treat this kind of situation. In the present study, inspired by the ideas proposed in Guo et al. (2002); Chun and Ladd (2007), a general extrapolation equilibrium boundary scheme is designed, namely only the equilibrium parts of Eq. (26) (the first two terms in the right hand of Eq. (26), namely Eq. (20)) should be extrapolated according to $\triangle$ as

$$F_2^{eq}(O,t) = \frac{2}{1+\triangle}\left[\alpha f_2^{eq}(W,t) + (1-\alpha) f_2^{eq}(B,t)\right] + \frac{\triangle - 1}{1+\triangle} f_2^{eq}(M,t),$$
$$G_2^{eq}(O,t) = \frac{2}{1+\triangle}\left[\alpha g_2^{eq}(W,t) + (1-\alpha) g_2^{eq}(B,t)\right] + \frac{\triangle - 1}{1+\triangle} g_2^{eq}(M,t), \tag{31}$$

when $0 < \triangle < 0.75$ and

$$F_2^{eq}(O,t) = \frac{1}{\triangle}\left[\alpha f_2^{eq}(W,t) + (1-\alpha) f_2^{eq}(B,t)\right] + \frac{\triangle - 1}{\triangle} f_2^{eq}(B,t), \tag{32}$$
$$G_2^{eq}(O,t) = \frac{1}{\triangle}\left[\alpha g_2^{eq}(W,t) + (1-\alpha) g_2^{eq}(B,t)\right] + \frac{\triangle - 1}{\triangle} g_2^{eq}(B,t),$$

when $0.75 \leqslant \triangle \leqslant 1$. The nonequilibrium parts $F_2^{neq}(O,t)$ and $G_2^{neq}(O,t)$ are still obtained by Eq. (25). Figs. 6 and 7 shows the variations of global error versus $1/\tau$ for different $\triangle$ with grid resolution 40×40. One can see the maximum of global error (defined in Eq. (30)) is less than 6% even when $\triangle$ is very small, which demonstrates the numerical stability and accuracy of the present scheme.

4.2. Micro-Couette flow with different wall temperatures

The second case is the micro-Couette flow with different wall temperatures. The temperature difference between the wall is determined by the Eckert Ec number, which is defined as:

$$\mathrm{Ec} = \frac{U_0^2}{c_p \triangle T} \tag{33}$$

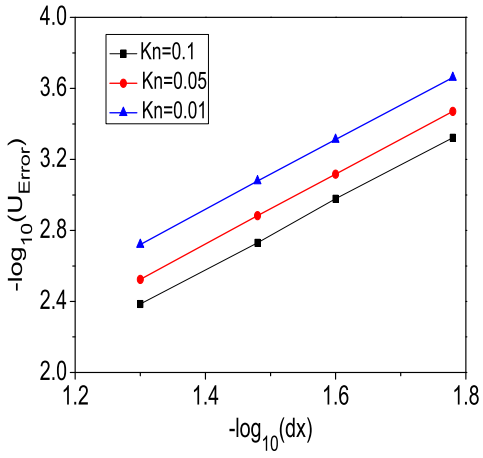

Fig. 4. Convergence behavior with different grid resolution and Kn.

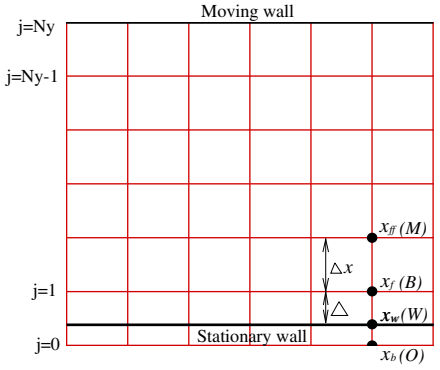

Fig. 5. The configuration of computational domain.

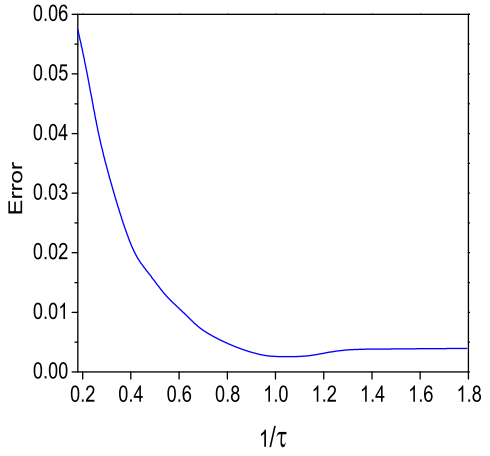

Fig. 6. Global error versus $1/\tau$: $\triangle = 0.2$.

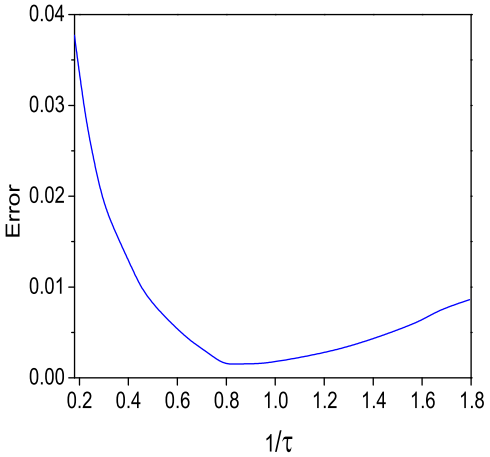

Fig. 7. Global error versus $1/\tau$: $\triangle = 0.9$.

$c_p = 1.0$ is the specific heat. Combined with $U_0 = 0.1c$ and the definitions of c and Ec, we can finally obtain the expression of c only related with Ec (Tian et al., 2006):

$$c = \frac{1}{\sqrt{\frac{1}{3} - \frac{0.005}{\mathrm{Ec}}}} \tag{34}$$

After c has been known, other parameters (such as U_0 and $\triangle T$) can be calculated out easily. Fig. 8 shows the dimensionless temperature profile at Ec = 1.0 with Kn = 0.01, 0.05, and 0.1, respectively. The temperature distribution is almost straight line because $\triangle T$ is relatively large and the influence of the viscous heat dissipation is relatively very small at low Ec. The wall temperature jump increases with the increasing of Kn. When Ec increases to 2.0, as shown in Fig. 9, the lines curve obviously. This results from the effect of viscous heat dissipation beginning to become notably. The temperature jump at the bottom wall is larger than that of Ec = 1.0 at the same Kn. While the temperature at top boundary is lower than that of Ec = 1.0 at the same Kn, which is more closer to the point of 1.0.

When the Ec increases to 3.0 in succession as illustrated in Fig. 10, we find that the fluid temperature near the top wall boundary is very close to 1.0 with different Kn. It means that the temperature jump at the top wall boundary is almost zero. When the Ec is 5.0, as shown in Fig. 11, the temperature at the upper part of the field is higher than that at the top boundary and the temperature jump on the top boundary is negative. The phenomena observed from the present scheme are in agreement with that in previous studies (Tian et al., 2006).

To test our scheme further, we simulate the case of larger Ec, which is illustrated in Fig. 12. The results are still in good agreement

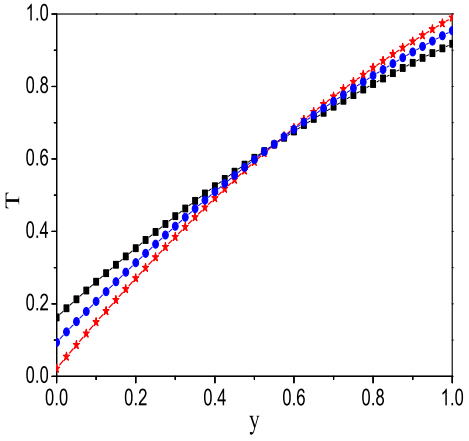

Fig. 8. Temperature profile of Ec = 1.0: solid line, analytical solution; pentacle, Kn = 0.01; dot, Kn = 0.05; square, Kn = 0.1.

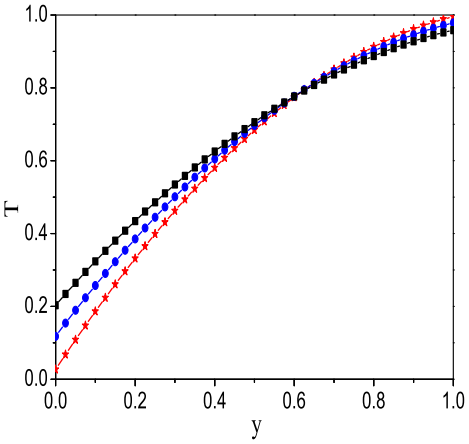

Fig. 9. Temperature profile of Ec = 2.0: solid line, analytical solution; pentacle, Kn = 0.01; dot, Kn = 0.05; square, Kn = 0.1.

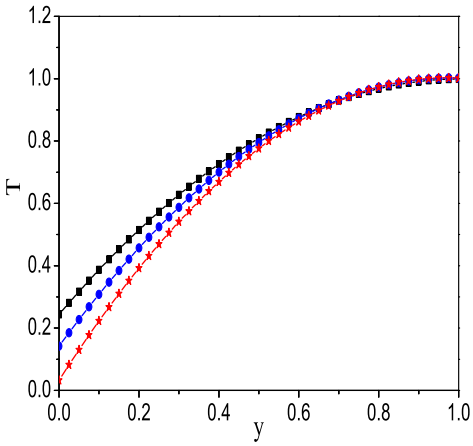

Fig. 10. Temperature profile of Ec = 3.0: solid line, analytical solution; pentacle, Kn = 0.01; dot, Kn = 0.05; square, Kn = 0.1.

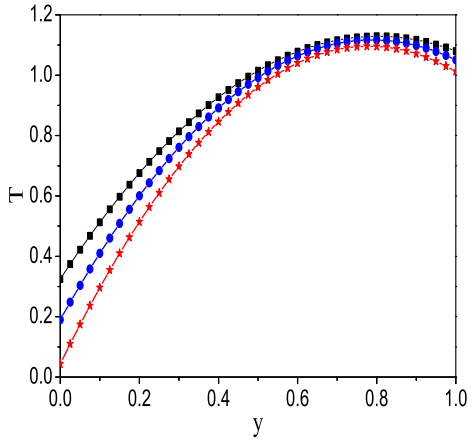

Fig. 11. Temperature profile of Ec = 5.0: solid line, analytical solution; pentacle, Kn = 0.01; dot, Kn = 0.05; square, Kn = 0.1.

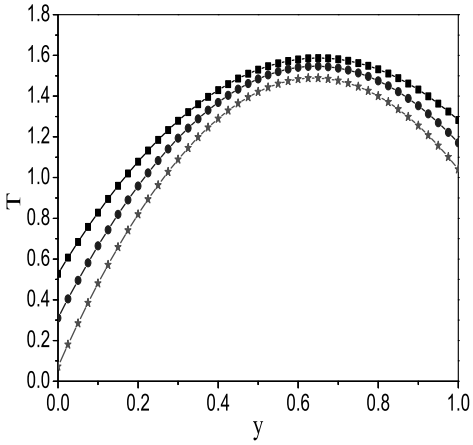

Fig. 12. Temperature profile of Ec = 10.0: solid line, analytical solution; pentacle, Kn = 0.01; dot, Kn = 0.05; square, Kn = 0.1.

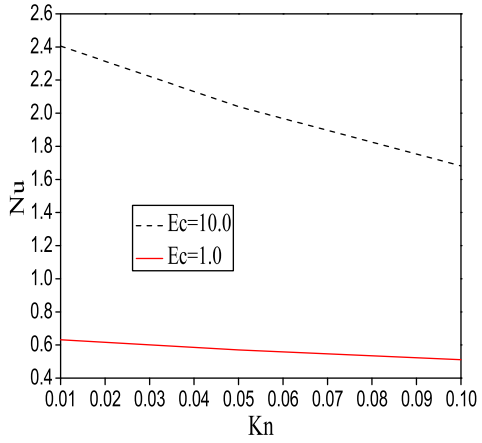

Fig. 13. Average Nusselt number Nu at the top wall versus Knudsen number Kn: dash line, Ec = 10.0; solid line, Ec = 1.0.

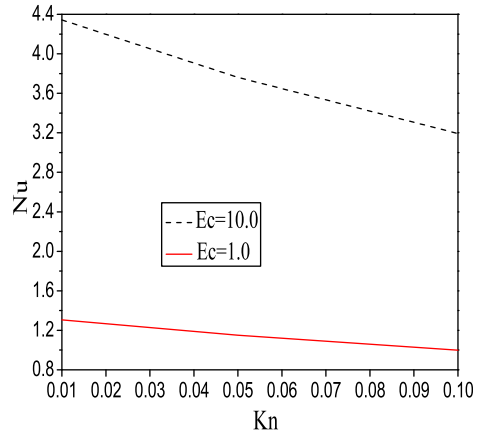

Fig. 14. Average Nusselt number Nu at the bottom wall versus Knudsen number Kn: dash line, Ec = 10.0; solid line, Ec = 1.0.

with the analytic results. It validates the capability of the present scheme for computing micro-flow with high Ec.

Figs. 13 and 14 illustrate the average Nusselt numbers (Nu) at the top and bottom walls, versus Kn, in which the cases Ec = 10.0 and Ec = 1.0 are chosen for the representatives. It can be seen that the heat transfer, represented by Nu, always decreases with increasing rarefaction. Therefore the Reynolds analogy is really preserved in the present scheme. From these two figures, it is also clear that the decrease of Nu with higher Ec is much faster than that with lower Ec.

5. Conclusion

In almost all existing studies using the LB method to investigate microfluidics, the popular Maxwell slip model is employed to capture the velocity slip and temperature jump. However, recently some debates on the shortcoming of Maxwell slip model were emergent and a good alternative, the Langmuir slip model, was developed as the remedy.

In the present study, we discuss how to implement the Langmuir slip model for the LB method to capture velocity slip and temperature jump in micro-flows with temperature difference. There are two obvious advantages of the present scheme: first, it has better physical relevancy, and some previous LB boundary schemes for macroscopic thermal flows can be naturally recovered from the present scheme when the Knudsen number $Kn \to 0$; second, the implementation of this scheme is straightforward.

The feasibility and the capability of the present scheme are explored by simulating thermal micro-Couette flows with different temperature boundary conditions. The numerical results agree well with the analytical solutions and the Reynolds analogy is preserved.

In the next work, we will validate its performance for curvilinear boundaries by simulating thermal micro-flows in circular pipes.

Acknowledgment

One of the present authors (Z. Tian) would acknowledge the support from the Research Foundation for Outstanding Young Teachers, China University of Geosciences.

References

Ansumali, S., Karlin, I.V., 2005. Consistent lattice Boltzmann method. Phys. Rev. Lett. 95, 260605.
Ansumali, S., Karlin, I.V., Frouzakis, C.E., Boulouchos, K.B., 2006. Entropic lattice Boltzmann method for microflows. Phys. A 359, 289305.
Chen, S., Doolen, G.D., 1998. Lattice Boltzmann method for fluid flows. Annu. Rev. Fluid Mech. 30, 329–364.
Chen, S., Krafczyk, M., 2009. Entropy generation in turbulent natural convection due to internal heat generation. Int. J. Therm. Sci. 48, 1978–1987.
Chen, S., Tian, Z., 2009. Simulation of microchannel flow using the lattice Boltzmann method. Physica A 388, 4803–4810.
Chen, S., Liu, Z., Zhang, C., et al., 2007. A novel coupled lattice Boltzmann model for low Mach number combustion simulation. Appl. Math. Comput. 193, 266–284.
Choi, H.I., Lee, D.H., Lee, D., 2005. Complex microscale flow simulations using Langmuir slip condition. Numer. Heat Transfer A 48, 407425.
Chun, B., Ladd, A.J.C., 2007. Interpolated boundary condition for lattice Boltzmann simulations of flows in narrow gaps. Phys. Rev. E 75, 066705.
Darhuber, A., Troian, S., 2005. Principles of microfluidic actuation by modulation of surface stresses. Annu. Rev. Fluid Mech. 37, 425–455.
Fillipova, O., Hanel, D., 1998. Grid refinement for lattice-BGK models. J. Comput. Phys. 147, 219–228.
Guo, Z., Zheng, C., Shi, B., 2002. An extrapolation method for boundary conditions in lattice Boltzmann method. Phys. Fluids 14, 2007–2010.
Guo, Z., Zheng, C., Shi, B., 2008. Lattice Boltzmann equation with multiple effective relaxation times for gaseous microscale flow. Phys. Rev. E 77, 036707.
He, X.Y., Chen, S.Y., Doolen, G.D., 1998. A novel thermal model for the lattice Boltzmann method in incompressible limit. J. Comput. Phys. 146, 282–300.
Ho, C., Tai, Y., 1998. Micro-electro-mechanical-systems (MEMS) and fluid flows. Annu. Rev. Fluid Mech. 30, 579–612.
Kao, P., Chen, Y., Yang, R., 2008. Simulations of the macroscopic and mesoscopic natural convection flows within rectangular cavities. Int. J. Heat Mass Transfer 51, 3776–3793.
Kim, S., Pitsch, H., 2008. Analytic solution for a higher-order lattice Boltzmann method: slip velocity and Knudsen layer. Phys. Rev. E 78, 016702.
Kim, H., Kim, D., Kim, W., Chung, P., Jhon, M., 2007. Langmuir slip model for air bearing simulation using the lattice Boltzmann method. IEEE Trans. Magn. 43, 2244–2246.
Kunert, C., Harting, J., 2007. Roughness induced boundary slip in microchannel flows. Phys. Rev. Lett. 99, 176001.
Kuo, L., Chen, P., 2008. A unified approach for nonslip and slip boundary conditions in the lattice Boltzmann method. Comput. Fluids. doi:10.1016/j.compfluid.2008.09.008.
Langmuir, I., 1933. Surface chemistry. Chem. Rev. 13, 147.
Lee, T., Lin, C.L., 2005. Rarefaction and compressibility effects of the lattice Boltzmann-equation method in a gas microchannel. Phys. Rev. E 71, 046706.
Lim, C.Y., Shu, C., Niu, X.D., Chew, Y.T., 2002. Application of lattice Boltzmann method to simulate microchannel flows. Phys. Fluids 14, 2299–2308.
Maxwell, J.C., 1879. On stresses in rarefied gases arising from inequalities of temperature. Philos. Trans. Roy. Soc. Lond. 170, 231–256.
Mei, R., Luo, L., Shyy, W., 1999. An accurate curved boundary treatment in the lattice Boltzmann method. J. Comput. Phys. 155, 307–330.
Myong, R.S., 2004. A generalized hydrodynamic computational model for rarefied and microscale diatomic gas flows. J. Comp. Phys. 195, 655–676.
Myong, R.S., Reese, J.M., Barber, R.W., Emerson, D.R., 2005. Velocity slip in microscale cylindrical Couette flow: the Langmuir model. Phys. Fluids 17, 087105.
Myong, R.S., Lockerby, D.A., Reese, J.M., 2006. The effect of gaseous slip on microscale heat transfer: an extended Graetz problem. Int. J. Heat Mass Transfer 49, 2502–2513.
Nie, X.B., Doolen, G.D., Chen, S.Y., 2002. Lattice-Boltzmann simulations of fluid flows in MEMS. J. Stat. Phys. 107, 279–289.

Niu, X., Hyodo, S., Munekata, T., Suga, K., 2007. Kinetic lattice Boltzmann method for microscale gas flows: issues on boundary condition, relaxation time, and regularization. Phys. Rev. E 76, 036711.

Reese, J.M., Gallis, M.A., Lockerby, D.A., 2003. New directions in fluid dynamics: non-equilibrium aerodynamic and microsystem flows. Philos. Trans. Roy. Soc. Lond., Ser. A 361, 2967–2988.

Shan, X., Yuan, X.F., Chen, H., 2006. Kinetic theory representation of hydrodynamics: a way beyond the Navier–Stokes equation. J. Fluid Mech. 550, 413–441.

Shi, Y., Zhao, T.S., Guo, Z., 2007. Lattice Boltzmann simulation of dense gas flows in microchannels. Phys. Rev. E 76, 016707.

Shu, C., Niu, X.D., Chew, Y.T., 2005. A lattice Boltzmann kinetic model for microflow and heat transfer. J. Stat. Phys. 121, 239–255.

Sofonea, V., Sekerka, R.F., 2005. Boundary conditions for the upwind finite difference lattice Boltzmann model: evidence of slip velocity in micro-channel flow. J. Comput. Phys. 207, 639–659.

Sofonea, V., Sekerka, R.F., 2005. Diffuse-reflection boundary conditions for a thermal lattice Boltzmann model in two dimensions: evidence of temperature jump and slip velocity in microchannels. Phys. Rev. E 71, 066709.

Succi, S., 2001. The Lattice Boltzmann Equation for Fluid Dynamics and Beyond. Oxford University Press, Oxford.

Succi, S., 2002. Mesoscopic modeling of slip motion at fluidsolid interfaces with heterogeneous catalysis. Phys. Rev. Lett. 89, 064502.

Szalmas, L., 2006. Slip-flow boundary condition for straight walls in the lattice Boltzmann model. Phys. Rev. E 73, 066710.

Tang, G., Tao, W., He, Y., 2005. Thermal boundary condition for the thermal lattice Boltzmann equation. Phys. Rev. E 72, 016703.

Tang, G.H., Gu, X.J., Barber, R.W., Emerson, D.R., Zhang, Y.H., 2008. Lattice Boltzmann simulation of nonequilibrium effects in oscillatory gas flow. Phys. Rev. E 78, 026706.

Tian, Z., Zou, C., Liu, Z., Guo, Z., Liu, H., Zheng, C., 2006. Lattice Boltzmann method in simulation of thermal micro-flow with temperature jump. Int. J. Mod. Phys. C 17, 603–614.

Tian, Z., Zou, C., Liu, H., Guo, Z., Liu, Z., Zheng, C., 2007. Lattice Boltzmann scheme for simulating thermal micro-flow. Physica A 385, 59–68.

Verhaeghe, F., Luo, Li-Shi, Blanpain, B., 2009. Lattice Boltzmann modeling of microchannel flow in slip flow regime. J. Comput. Phys. 228, 147–157.

Wang, C.H., Yang, R., 2006. A numerical study for slip flow heat transfer. Appl. Math. Comput. 173, 1246–1264.

Zhang, Y.H., Qin, R.S., Emerson, D.R., 2005. Lattice Boltzmann simulation of rarefied gas flows in microchannels. Phys. Rev. E 71, 047702.

Zhang, Y.H., Gu, X.J., Barber, R.W., Emerson, D.R., 2007. Modelling thermal flow in the transition regime using a lattice Boltzmann approach. Europhys. Lett. 77, 30003.